Comparative study of switching controls in vibration and acoustic noise reductions for switched reluctance motor

J.Y. Chai, Y.W. Lin and C.M. Liaw

Abstract: A comparative study of vibration and acoustic noise reductions via electronic switching controls for switched reluctance motor (SRM) is presented. First, studies concerning the acoustic noise and vibration sources, their effects and the existing mitigation approaches are given. Then five switching control approaches, which belong to the magnetic and electronic remedies, are proposed and applied to the established SRM drive to comparatively evaluate their effectiveness and limitations. These approaches include random frequency pulse width modulation with harmonic spectrum shaping, turn-on and turn-off angles advanced shift with fixed dwell angle, randomising turn-off angle, current-tail profiling without and with advancing commutation shift. The theoretical basis, implementation and performance evaluation of each approach are presented in detail. Comparative evaluation shows that the hybrid approach combining the current-tail profiling and the commutation advancing can yield the best compromise performance in vibration reduction, acoustic noise reduction and improved energy conversion efficiency.

1 Introduction

Similar to the variable reluctance stepping motor, the switched reluctance motor (SRM) belongs to a doubly-salient and singly-excited machine [1–3]. It possesses a lot of inherent structural advantages, such as rigid structure, high power density, high reliability, low maintenance requirement and suited for high-temperature and high-speed operations. In addition, its converter is free from arm fed-through short circuit. However, the SRM also suffers from many disadvantages: (i) high torque ripple; (ii) high acoustic noise and vibration; (iii) absolute rotor position information is required for performing the converter switching for the SRM; (iv) nonlinear winding inductance and torque generating characteristics.

In dealing with the mechanical vibration and acoustic noise problems of an SRM, there has been much current work [4–19] concerning their origin, exploration and reduction. The studies in [2, 4–12] show that the sources of acoustic noise can be basically classified into four categories, namely magnetic, mechanical, aerodynamic and electronic. Among these, it is shown that the radial attractive force between stator and rotor is the dominant one, particularly for the case in which the de-energisation occurs at the aligned rotor position. In making performance evaluation, it was found that vibration measurement can be used as an alternative to acoustic noise [4].

Basically, the existing solutions for vibration and acoustic noise reduction can be achieved via the motor design [5–7] and the converter control. Some typical research areas of the former topic are: (i) the use of thicker back-iron, wherein the trade-off between noise and power density must be considered; (ii) applying an axial preload to reduce bearing noise; (iii) dynamic rotor balancing to eliminate noise due to rotor unbalance; (iv) the adoption of a slightly larger airgap; and (v) suitable core laminations; in [6, 7] the finite-element method is used for computer-aided analysis and design.

As to the converter control approaches, there exist three key tunable parameters, namely the turn-on angle, the turn-off angle and the current shape. In the research reported in [8], the optimised current profile including turn-on and turn-off angles is generated using an artificial neural network to yield performance compromise between acoustic noise, efficiency and average torque. As generally recognised, winding current-tail shaping is an effective means, which has been accomplished via voltage smoothing, and two-stage and three-stage commutation control [4, 9, 10, 12]. Random PWM (RPWM) switching control [13, 14] and random turn-on and turn-off angles [15] have also been studied recently. However, owing to limited success, the optimisation of the key parameters in random switching schemes needs to be studied more deeply [13]. Accordingly, vibration reduction using random frequency PWM (RFPWM) with harmonic spectrum shaping is presented in this paper.

Recently in [16], a hybrid excitation method was presented. Overlap excitation is employed to reduce the rapid change of radial MMF, and a C-damp converter is added to reduce the decrease in efficiency. In [17], prediction and experimental transfer function estimation of the vibration caused by the magnetic force are presented, and accordingly a vibration reduction control strategy is proposed. Intuitively, minimisation of ripple torque is a direct means, and this type of research is reported in [18–22]. In [18], the ripple torque reduction is achieved via torque nonlinear control, associated with a suitable phase commutation strategy. In [19], the current waveforms are

IEE Proceedings online no. 20050340

doi:10.1049/ip-epa:20050340

Paper first received 1st May and in final revised form 24th November 2005

The authors are with the Department of Electrical Engineering, National Tsing Hua University Hsinchu, Taiwan, Republic of China

E-mail: cmliaw@ee.nthu.edu.tw

optimised using computer search techniques to yield ripple-free torque. In [21], torque ripple minimisation is obtained by optimum harmonic current injection, and in [22] the same authors developed the online simplex optimisation technique to set the injected current harmonics, and it has been verified to be effective in reducing steady-state torque ripple. Each approach described above possesses its advantages and limitations in implementation and effectiveness. In this paper, reductions of vibration and acoustic noise are achieved via commutation tuning, random switching and current profiling approaches and also their combination.

In this paper, a DSP-based SRM drive with the necessary sensors and interfacing circuits is first constructed. The tuning and RPWM schemes for performing the required studies are also established. Then the sources of acoustic noise and vibration of an SRM are included to facilitate the development of these approaches. According to the phenomena being observed, five mitigation approaches for acoustic noise and vibration have been developed and their performances are comparatively evaluated. These approaches include random frequency PWM with harmonic spectrum shaping, commutation advanced tuning, turn-off instant randomisation, and current-tail profiling without and with commutation advancing shift. The last hybrid method, which combines current-tail profiling and commutation advancing, is the most effective means in yielding a compromise performance in vibration reduction and torque generating capability. Theoretical bases and implementations of all the proposed schemes are described in detail, and their performances are evaluated experimentally.

2 Sources of vibration and acoustic noise

Although there are many inherent structural advantages, the doubly-salient structure and non-ideal switched square-wave winding current give the SRM higher torque ripple, and thus lead to the generation of higher vibration and acoustic noise. In addition, the rotor position and current-dependent winding nonlinear inductance makes its torque and dynamic behaviour highly nonlinear. Moreover, analysis of vibration behaviour is also difficult to perform accurately. For performing the development of key technologies, it is indispensable to understand thoroughly the key features of an SRM. In this Section, the governing equations of an SRM are first introduced, and then the sources of vibration and acoustic noise are considered.

2.1 Governing equations

2.1.1 Voltage equation: By neglecting the coupling effect between phases, the voltage equation of a particular phase winding can be expressed by:

$$v = Ri + \frac{d\lambda(i,\theta_r)}{dt} = Ri + L(\theta_r)\frac{di}{dt} + e(i,\theta_r,\omega_r) \qquad (1)$$

where v = winding terminal voltage, i = winding current, R = winding resistance, $L(\theta_r) \triangleq \partial\lambda(i,\theta_r)/\partial i$ = incremental winding inductance, and $e(i,\theta_r,\omega_r) \triangleq [\partial\lambda(i,\theta_r)/\partial\theta_r]$ $(d\theta_r/dt)$ = back electromagnetic force (EMF). The per-phase converter-fed equivalent circuit corresponding to (1) is shown in Fig. 1*a*.

Observation: As shown in Fig. 1*a*, the winding current is established via PWM switching control of the power converter. The non-ideal square-wave shape winding current generally results in larger torque ripple compared with other types of motors. As the speed increases, the current will even become single-pulse type.

2.1.2 Torque equation: By assuming the linear magnetic system and neglecting the coupling effect between phases, the developed torque $T_{ei}(i)$ per phase can be derived from its energy or coenergy $W_c(\theta_r)$ as follows:

$$T_{ei}(i) = \left[\frac{\partial W_c(\theta_r)}{\partial\theta_r}\right]_{i=\text{constant}} = \frac{\partial\frac{1}{2}L(\theta_r)i^2}{\partial\theta_r} = \frac{1}{2}i^2\frac{\partial L(\theta_r)}{\partial\theta_r} \triangleq K_t(\theta_r)i^2 \qquad (2)$$

where $K_t(\theta_r) \triangleq \frac{1}{2}\partial L(\theta_r)/\partial\theta_r$ denotes the torque generation constant.

The composite generating torque T_e and mechanical equation of an SRM can be derived by summing the torques produced by all phases:

$$T_e(i) = \sum_{i=1}^{4} T_{ei}(i) = T_L + B\omega_r + J\frac{d\omega_r}{dt} \qquad (3)$$

where T_L = load torque, J = moment of inertia and B = damping ratio. The control system block diagram corresponding to (3) is shown in Fig. 1*b*, where I_c = current command magnitude, and $H_i(s)$ denotes the ith phase current hypothesised tracking transfer function. The typical composite developed torque pattern of an SRM is shown in Fig. 1*c*.

Observation: As far as the switching control of winding current is concerned, some comments are:

- The current and torque waveforms given in Figs. 1*b* and *c* show that without special current waveform profiling, in addition to the torque ripple yielded by each phase due to its non-ideal current waveform, large commutation ripples also result because of the notch between adjacent phases.
- The extent of vibration generation depends on vibration mode frequencies and the frequency components in the torque ripples, which are affected by speed and current waveform.
- Torque ripple is considered to be one of the major sources of vibration and acoustic noise. Some suitable switching control and commutation tuning approaches can be employed for effectively reducing this noise.

2.2 Sources of acoustic noise and vibration

As mentioned in Section 1, there are basically four types of acoustic and vibration sources. Only two of these relate to the studies reported in this paper and they are discussed below.

2.2.1 Magnetic sources: For the SRM shown in Fig. 2 with a particular phase winding being excited, the generated magnetic flux across the airgap produces radial forces on the stator and rotor, and thus results in magnetic noise and vibration. To simplify the derivation, it is assumed that: (i) the magnetic circuit is linear; and (ii) the reluctance of iron is neglected. Referring to the configuration of motor structure shown in Fig. 2, one can find the airgap flux density at the overlap angle θ [1]:

$$B_g(\theta,g,i) = \mu_o H_g = \frac{\phi}{lr\theta} = \mu_o\frac{Ni}{g} \qquad (4)$$

where θ = overlap angle between stator and rotor, g = airgap length between stator and rotor at overlap, r = rotor outer radius, l = iron axial length and N = number of turns per phase winding. Since θ is determined by the

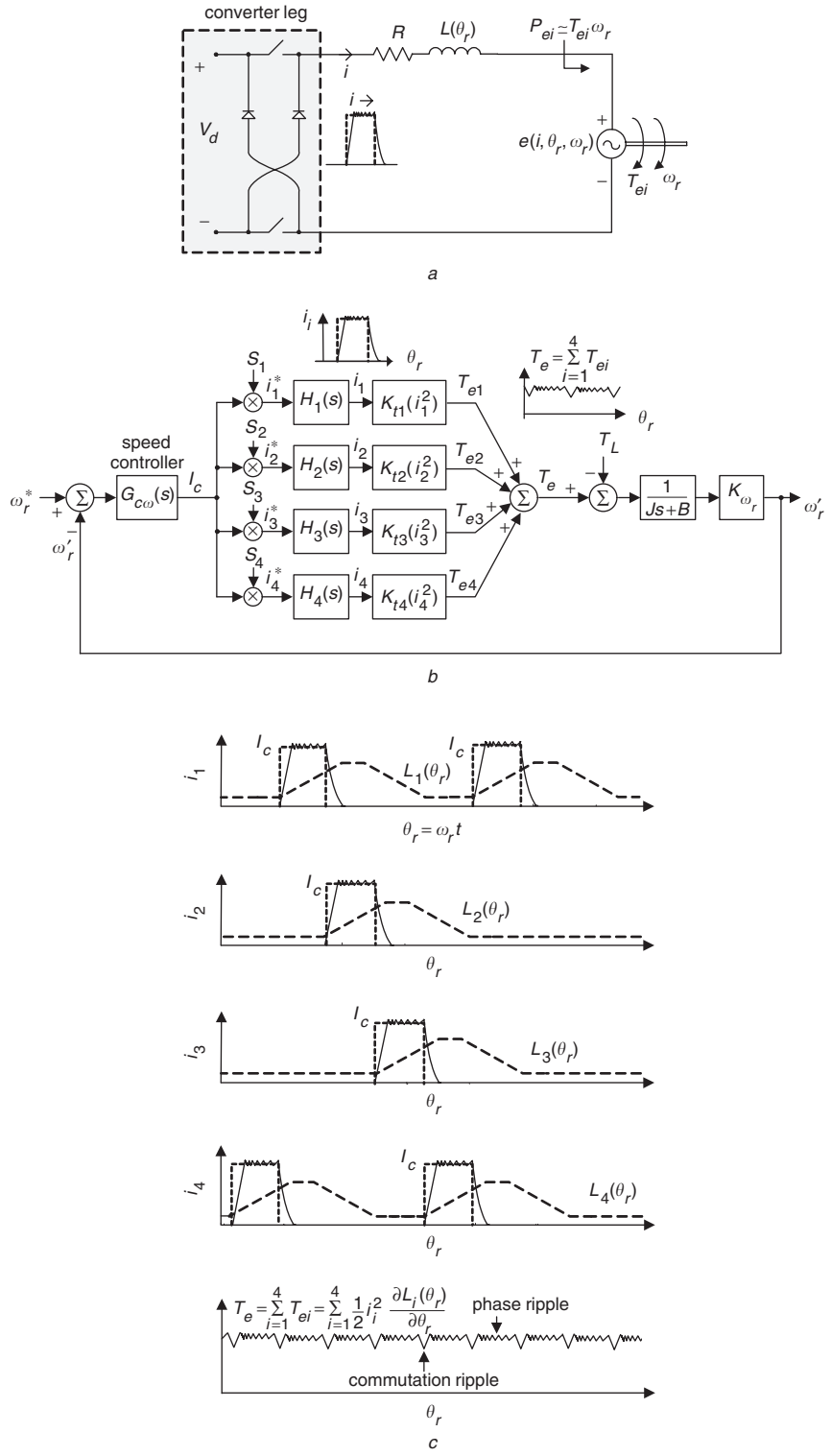

Fig. 1
a Per-phase converter-fed winding equivalent circuit
b Composite torque generating scheme and mechanical dynamic model
c Inductance, winding currents and composite developed torque at medium speed

rotor position θ_r, B_g is also a nonlinear function of θ_r, i.e. $B_g = B_g(\theta_r, g, i)$, and the corresponding flux $\phi(\theta, g, i) = B_g(\theta, g, i) lr\theta$.

From Fig. 2, one can derive the incremental electrical energy of the excited winding:

$$dW_e = id\lambda = \frac{g}{\mu_o lr} \frac{\phi}{\theta} d\phi \tag{5}$$

The magnetic field stored energy can be expressed as:

$$W_s(\theta, g, i) = \frac{g}{2\mu_o lr} \frac{\phi^2}{\theta} \tag{6}$$

By neglecting all electrical and magnetic losses, one can find $dW_e = dW_s + dW_m$ from the energy balance relationship. And then the incremental magnetic field energy corresponding to the change of θ on the excited phase winding can be

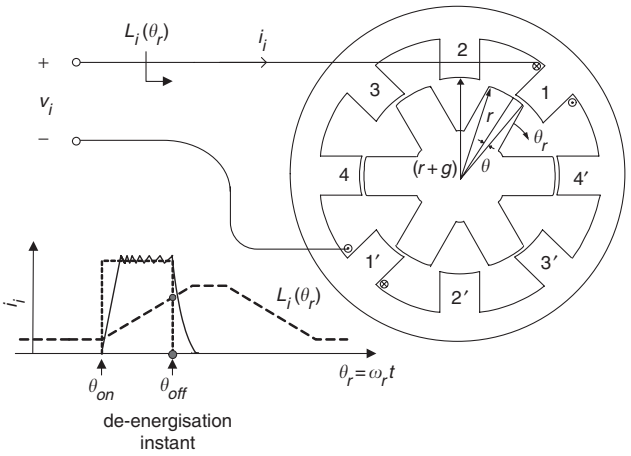

Fig. 2 *Relevant dimensions and geometrical parameters between rotor and stator teeth for particular excited phase winding*

derived from (6) as [1]:

$$dW_s = -dW_m + dW_e = \frac{-g}{2\mu_o lr}\frac{\phi^2}{\theta^2}d\theta + \frac{g}{\mu_o lr}\frac{\phi}{\theta}d\phi \qquad (7)$$

Tangential force:

From (5) and (7), the incremental mechanical energy is:

$$dW_m = \frac{g}{2\mu_o lr}\frac{\phi^2}{\theta^2}d\theta \qquad (8)$$

Then, the electromagnetic tangential torque and thus force can be derived as:

$$F_t = \frac{T_e}{r} = \frac{\partial W_m/\partial\theta}{r} = \frac{gl}{2\mu_o}B^2(\theta, g, i) \qquad (9)$$

Radial force:

Similarly, the incremental magnetic field energy corresponding to the change of g can be derived from (6) as:

$$dW_s = \frac{1}{2\mu_o lr}\frac{\phi^2}{\theta}dg + \frac{g}{\mu_o lr}\frac{\phi}{\theta}d\phi \qquad (10)$$

Then dW_m and thus the radial force F_n can be found from (5) and (10) as:

$$F_n = \frac{\partial W_m}{\partial g} = -\frac{1}{2\mu_o lr}\frac{\phi^2}{\theta} = -\frac{lr\theta}{2\mu_o}B^2(\theta, g, i) \qquad (11)$$

Thus, the ratio between radial and tangential forces is obtained from (9) and (11):

$$\frac{F_n}{F_t} = -\frac{r\theta}{g} \qquad (12)$$

Observation: Equation (12) indicates that the radial force in an SRM is proportional to the overlap angle θ and it has an impact on the machine. Its effect is cancelled through the rotor and stator bodies, subject to the generation of vibrations. During driving operation, the largest F_n and hence vibration and acoustic noise will be generated at the de-energisation instant of a particular phase occurring at the aligned position. This fact can be used as a rough guide to find suitable remedies, for example, the advanced commutation shift will let the overlap angle θ decrease at the de-energisation instant.

2.2.2 Electronic sources: The winding current harmonic is a major factor. Additionally, the winding current waveform and thus the flux linkage during each switching operation vary significantly with time. Some features concerning these vibration sources are [1, 3, 4]:

(i) At a given rotor position with the same current magnitude, the single-pulse mode may induce a higher peak vibration than the current-chopping mode. And in current-chopping mode, a higher current-change rate causes larger vibrations. Obviously, the higher current magnitude induces larger vibrations.

(ii) Vibrations are larger during the turn-off process owing to the higher current-chopping rate occurring near the aligned position where the maximum vibration is caused by the radial force between stator and rotor. Turn-off before full alignment position may reduce vibrations. However, some negative phenomena will result, and the compromise considerations should be taken into account. These issues will be treated in detail later in this paper.

(iii) For a four-phase 8/6 SRM, the vibrations in a stator pole lagging 90° from the excited pole are out of phase with the vibrations of the excited pole. The largest vibrations may occur when the ripple frequencies of the winding current coincide with the resonant frequencies of the stator. Random PWM switching control [23] with proper spectrum shaping [24] may be an effective remedy. This control strategy will be studied in this paper.

3 Established DSP-based SRM drive and problem statement

3.1 DSP-based SRM drive

The power circuit and the established DSP-based SRM drive are shown in Figs. 3*a* and *b*. It mainly consists of an SRM, a $2(n+1)$ switch Miller's converter and a DSP control board. While the switches S_1–S_4 are in charge of commutation, S_A and S_B are used for performing the PWM switching control for four phase windings. The SRM employed in this paper is manufactured by TASC Drives Ltd., and is four-phase 8/6 pole with the ratings of 400 V, 1500 rpm, 4 kW. The measured stator winding resistance R is 0.96 Ω, and the inductance varies between 14 and 125 mH. The DC-link voltage is set as $V_d = 400$ V. A permanent-magnet synchronous generator with resistive load R_L serves as the dynamic load of the SRM. The DSP ADMC401 manufactured by Analog Devices Co. is employed to build up the digital control environment. The PWM switching control signals are generated directly by the PWM modulator in the DSP. Ramp-comparison current-controlled PWM (RC CCPWM) schemes with fixed and random switching frequencies are designed, and commutation tuning is achieved by modifying the commutation signals for S_1–S_4.

3.2 Problem statement

In this paper, magnetic and electronic remedies for reducing vibration and acoustic noise of an SRM drive are proposed and comparatively evaluated for their effectiveness. The RFPWM, an electronic approach, is used for randomising the harmonic spectral distribution of phase winding current. This is achieved digitally in the DSP by the developed PWM modulator and RFPWM scheme shown in Fig. 3*b*.

As to the magnetic means, four approaches are studied in this paper, these include (i) simultaneous advancing shift of turn-on and turn-off angles; (ii) randomising turn-off angle;

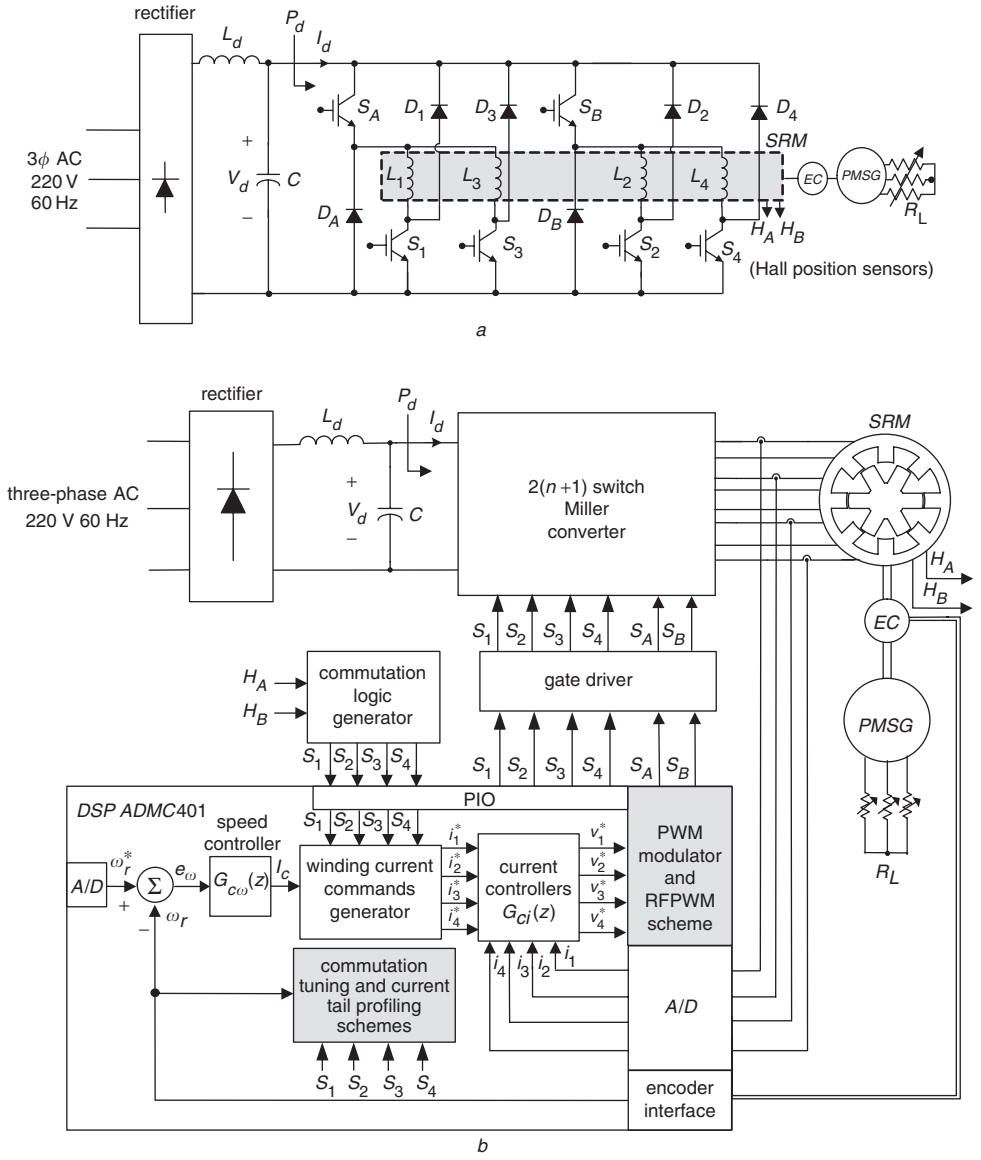

Fig. 3 *Developed SRM drive*
a Power circuit
b DSP-based control scheme

(iii) current-tail profiling; and (iv) current-tail profiling with advancing commutation shift. All these tasks are accomplished by the commutation tuning and current-tail profiling schemes shown in Fig. 3*b*. Details concerning the analysis, design and realisation of all the proposed control schemes are presented in the next Section.

4 Proposed vibration and acoustic noise reduction approaches

4.1 Random PWM switching and harmonic spectrum shaping

4.1.1 Intuitive spectral analysis: The key to this method is to vary the winding current PWM switching frequency randomly, such that its harmonic spectrum can be uniformly distributed. It follows that the effects of harmonics on the acoustic noise and vibration are reduced. Among the existing random PWM techniques [13, 14, 23, 24], the random frequency PWM (RFPWM) is the simplest one. In an RFPWM scheme, the frequency of its triangular carrier $v_{tri}(t)$ is randomly changed according to the employed random signal $r(t)$. The basic concept of this approach can be understood from Fig. 4*a*. The frequency of $v_{tri}(t)$ is set to be:

$$f_s = f_{s0} + r(t)\Delta f_s \tag{13}$$

where f_s = instant switching frequency, f_{s0} = average switching frequency, Δf_s = switching frequency variation magnitude, and $r(t)$ = uniformly distributed random numbers in the range of $[-1, +1]$. In Fig. 4*b*, $\underline{f}_h$ and $\overline{f}_h$ denote the lowest and highest harmonic frequency components of winding current i_i due to RFPWM, and $\Delta f_c \triangleq \underline{f}_h - \overline{f}_1$ is the frequency range within which the current harmonics should be attenuated as far as possible [23, 24].

By randomly varying the triangular carrier frequency, the harmonic spectrum in winding current i'_1 (taking the first phase winding as an example) under RC CCPWM control can be made to be uniformly distributed, as shown in Fig. 4*b*. Realisation of the RFPWM scheme using an analogue circuit is tedious. In this paper, the DSP-based digital RFPWM control algorithm is developed.

Comments: For a fixed switching frequency standard PWM scheme, one can choose the switching frequency to be higher than about 20 kHz (ultrasonic frequency) to reduce

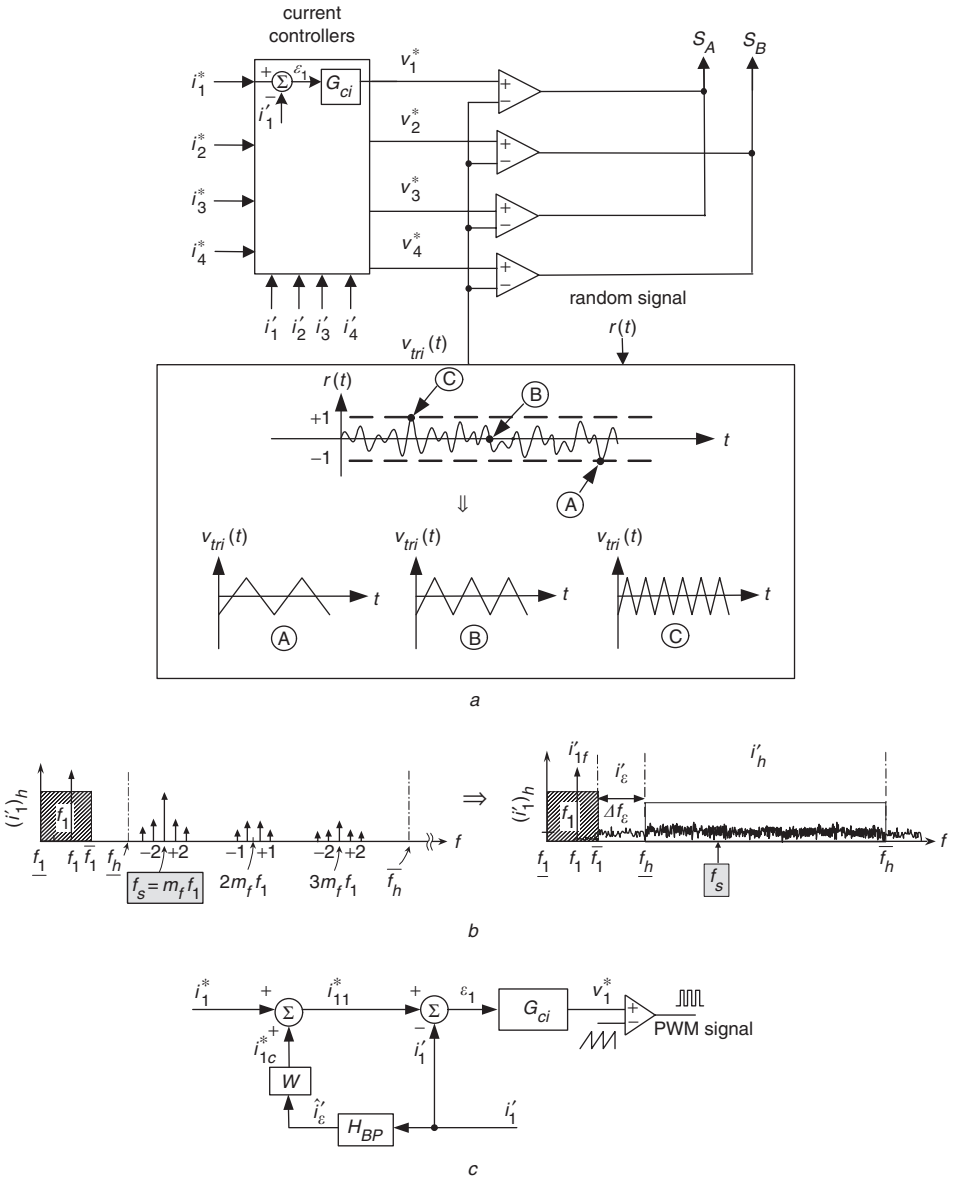

Fig. 4
a Proposed random PWM modulator
b Resulting harmonic spectra
c Proposed harmonic spectrum shaping scheme (per phase)

the acoustic noise. However, this is not helpful for the vibration reduction of an SRM, since its dominant vibration frequency is normally located far below the switching frequency. On the other hand, the key purpose of applying RFPWM is to let the harmonic spectrum be uniformly distributed, and thus the possibility and extent of vibration caused by the current harmonics with coincided frequencies can be reduced. However, similarly, the effectiveness of vibration reduction by RFPWM is also not very significant [13]. The chief reason lies in the harmonics with frequencies within Δf_ε (in which the dominant vibration frequency is located) in Fig. 4*b* not being able to reduce via standard RFPWM [23]. The improvement is made as follows.

4.1.2 Robust harmonic spectrum shaping:

For the four-phase 8/6 SRM employed in this paper, the vibration frequency range found from measurement is around 1.43 kHz. To allow the RFPWM be more effective in vibration reduction, the robust spectrum shaping technique [24] is employed here. The proposed RFPWM scheme with robust harmonic spectrum shaping is shown in Fig. 4*c*. A bandpass filter is employed to extract the current harmonics within the frequency range $\Delta f_\varepsilon = 0.93$–$1.93$ kHz (centre frequency $f_0 = 1.43$ kHz) from the winding current, and then a compensation control signal $i^*_{1c} = W(\hat{i}'_\varepsilon)$ attenuates the harmonics to within Δf_ε.

Robustness analysis: Taking the first phase winding as an example, let the PWM switching controlled winding current i'_1 shown in Fig. 4*b* be modelled as:

$$i'_1 \triangleq H_i i^*_1 \triangleq i'_{1f} + i'_\varepsilon + i'_h \tag{14}$$

where H_i denotes an assumed winding current tracking transfer function as described previously, i'_{1f}, i'_ε and i'_h represent the current components in the fundamental frequency range, Δf_ε and high harmonic frequency range, respectively. Suppose that the component i'_ε within Δf_ε can be perfectly extracted by the bandpass filter (i.e. $\hat{i}'_\varepsilon \simeq i'_\varepsilon$) from Fig. 4*c*; one can derive:

$$i'_1 = i'_{1f} + i'_\varepsilon + i'_h = H_i(i^*_1 + W\, i'_\varepsilon) \tag{15}$$

And thus the winding current after applying robust spectrum shaping control becomes:

$$i'_1 = H_i i^*_1 = i'_{1f} + (1 - H_i W) i'_\varepsilon + i'_h \tag{16}$$

Hence, the current i'_ε within Δf_ε has been reduced by a factor of $(1 - H_i W)$.

4.1.3 Implementation of proposed random switching scheme and spectrum shaping scheme:

For a standard PWM mechanism, its switching frequency is fixed and determined according to the program setting. The PWM timer, which is clocked at the DSP instruction rate, controls the internal operation of the PWM modulator. The content (called PWMTM) is set in a 16-bit PWMTM register and used to control the PWM switching frequency. By randomly changing the content in the 16-bit PWMTM register, which has 32 768 variations, according to the random variable $r(t)$, the switch frequency can be randomised. In this study, $f_{s0} = 10\,\text{kHz}$ and $\Delta f_s = 5\,\text{kHz}$ are set.

The key parameters and transfer functions in Fig. 4*c* are chosen to be $W = 0.9999$, $_{HBP}(s) = 6.29 \times 10^3 s/(s^2 + 6.29 \times 10^3 s + 80.73 \times 10^6)$ (centre frequency $f_0 = 1.43\,\text{kHz}$, quality factor $Q = 1.428$, bandwidth $= f_0/Q = 1.0\,\text{kHz}$), $G_{ci}(s) = 30 + 8000/s$. The proposed spectrum shaping scheme shown in Fig. 4*c* is realised digitally in the DSP. All the continuous transfer functions are transformed to the discrete-time domain using the bilinear z-transform. The sampling interval T_i is chosen to be 0.1 ms.

4.1.4 Experimental results:

With $\omega_r = 700\,\text{rpm}$, $R_L = 158\,\Omega$, $P_d \simeq 1.6\,\text{kW}$, Fig. 5*a* shows the measured winding current waveforms of the SRM drive and their spectra by fixed switching frequency standard PWM ($f_s = 10\,\text{kHz}$) and RFPWM ($f_s = 5$–$15\,\text{kHz}$) schemes. The uniform harmonic spectrum due to RFPWM can be observed from the result. Figure 5*b* shows the current waveforms and their spectra by RFPWM without and with robust harmonic spectrum shaping. One can find from the results that the harmonics within the frequency range $\Delta f_\varepsilon = 0.93$–$1.93\,\text{kHz}$ have been greatly attenuated. The reduction of vibration is evaluated by the measured acceleration, which is measured by an accelerometer, manufactured by Wilcoxon Research Company, USA, being mounted midway in the stator frame. The measured accelerations corresponding to the cases of Figs. 5*a* and *b* are compared in Fig. 5*c*. One can observe from Fig. 5*c* that, through applying the proposed harmonic spectrum shaping technique, the vibration reduction by RFPWM can be improved, although its effectiveness has been considered to be limited until now. The chief reason lies in the fact that the probability of coincidence of winding current ripple frequencies with the stator resonant frequencies is reduced. Further comparison between the winding current waveforms shown in Figs. 5*a* and *b* also shows that lower current magnitude and smaller changing rate at turn off are obtained by the RFPWM with spectrum shaping, which is equivalent to the current-tail profiling technique presented in Subsection 4.4.

At another operation condition ($\omega_r = 1500\,\text{rpm}$, $R_L = 104\,\Omega$, $P_d \simeq 2.2\,\text{kW}$), the measured accelerations by standard PWM, RFPWM and RFPWM with shaping are shown in Fig. 5*d*. The same phenomena in vibration reduction can also be observed. Although the measured results at larger loads are not provided because of the rating limit of the dynamic load, the effectiveness of the proposed vibration reduction approach will also be predictable.

4.2 Commutation advanced shift

The main problem of acoustic noise and vibration generation in an SRM lies in the winding being turned off around the aligned position with maximum radial force. It is known that commutation tuning is an effective means of improving the torque generating characteristics of an SRM, including the maximum, RMS and ripple torques. There are many tunable variables and tuning approaches in this area. As far as the acoustic noise and vibration reduction are concerned, the advanced shift of turn-off angle is effective and commonly employed. Figure 6*a* shows the idealised winding current and inductance profiles of a particular phase under the simultaneous shift of θ_{on} and θ_{off} with fixed dwell angle θ_d.

Comments:

(i) With the commutation advanced shift, it can be seen clearly from Fig. 6a that the overlap angle between stator and rotor is decreased, so the radial force at turn-off can be reduced from (11) and (12).

(ii) The advanced shift can also lead to a quicker winding current buildup, and thus the commutation torque ripple and vibration are reduced accordingly. The research reported in [25] indicated that the advanced shift angle θ_{o1} shown in Fig. 6a to enable the winding current to be linearly raised to its command I_c is:

$$\theta_{o1} \triangleq \theta_{on} - \theta'_{on} = \frac{L_{\min} I_c \omega_r}{V_d} \tag{17}$$

Let the SRM operate at $\omega_r = 700\,\text{rpm}$, $R_L = 158\,\Omega$. The measured vibrations are compared in Fig. 6*b* and the results indicate that, through applying the commutation advanced shift, the stator vibration is greatly reduced. The results (not shown here) also show that the magnitude of the current command is reduced from $I_c = 4.5$ to 2.5 A by the proposed approach. For another operating condition ($\omega_r = 1500\,\text{rpm}$, $R_L = 104\,\Omega$), the measured vibrations are shown in Fig. 6*c*. The results of Fig. 6*c* also show that the reduction of vibration at higher speed can be effectively achieved by commutation advanced shift.

4.3 Randomised turn-off angle

The randomised turn-on and turn-off angles to reduce the vibration and acoustic noise has been studied in [4, 15]. Since the turn-off angle is the key variable relating to the vibration, only the randomised turn-off angle is considered here. In the proposed tuning control approach shown in Fig. 7*a*, the turn-on angle θ_{on} is fixed and the turn-off angle θ_{off} is randomly varied around the average value according to:

$$\theta'_{off} = \theta_{off} + r(t)\Delta\theta \tag{18}$$

where θ_{off} = original or average turn-off angle, θ'_{off} = the varied turn-off angle, $\Delta\theta$ = magnitude of turn-off angle variation, and $r(t)$ = uniformly distributed random numbers with its magnitude being varied in the range of $[-1, +1]$.

Comments: From (11), (12), Fig. 2 and Fig. 7*a*, one can find that the equivalent overlap angle θ is reduced owing to randomising θ_{off} It follows that the vibration is reduced accordingly. However, if the turn-on angle is fixed and the turn-off angle is advanced, the conduction period of the winding current and thus the torque generating capability will decrease. On the other hand, if the turn-off angle is reduced too much, the current-tail flowing in the decreasing inductance region may result in negative torque. It follows from the above observations that too large a value of $\Delta\theta$ should be avoided in order to avoid the sacrifice of

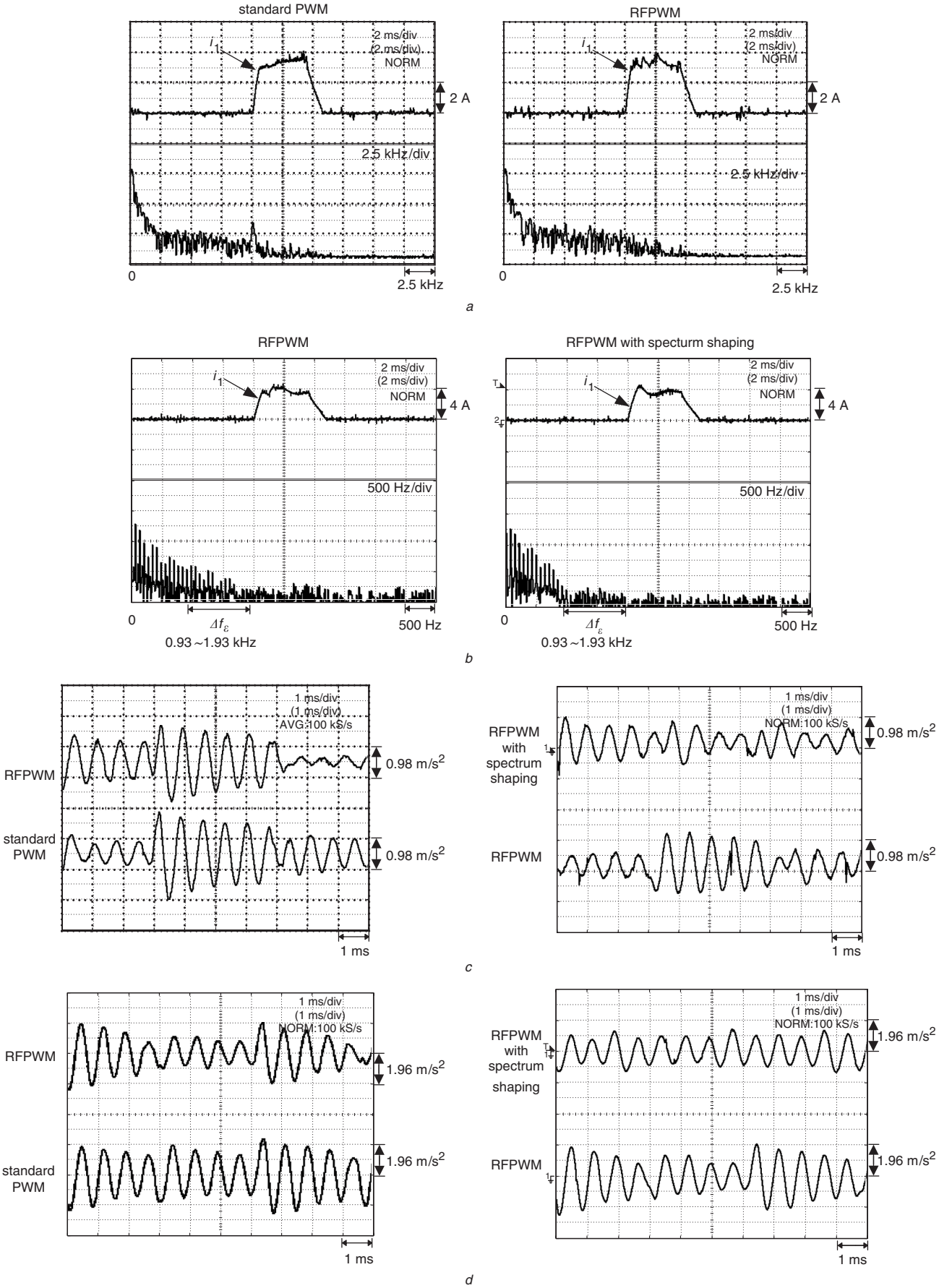

Fig. 5

a Measured winding current waveforms and their spectra by fixed frequency (standard) PWM ($f_s = 10\,\text{kHz}$) and proposed RFPWM ($f_s = 5$–$15\,\text{kHz}$) scheme at $\omega_r = 700\,\text{rpm}$, $R_L = 158\,\Omega$

b Measured waveforms and spectra of winding currents by proposed RFPWM without (left) and with (right) robust harmonic spectrum shaping schemes at $\omega_r = 700\,\text{rpm}$, $R_L = 158\,\Omega$

c Measured accelerations by standard SPWM, RFPWM without and with robust harmonic spectrum shaping schemes at $\omega_r = 700\,\text{rpm}$, $R_L = 158\,\Omega$

d Measured accelerations by same schemes as *c* at $\omega_r = 1500\,\text{rpm}$, $R_L = 104\,\Omega$

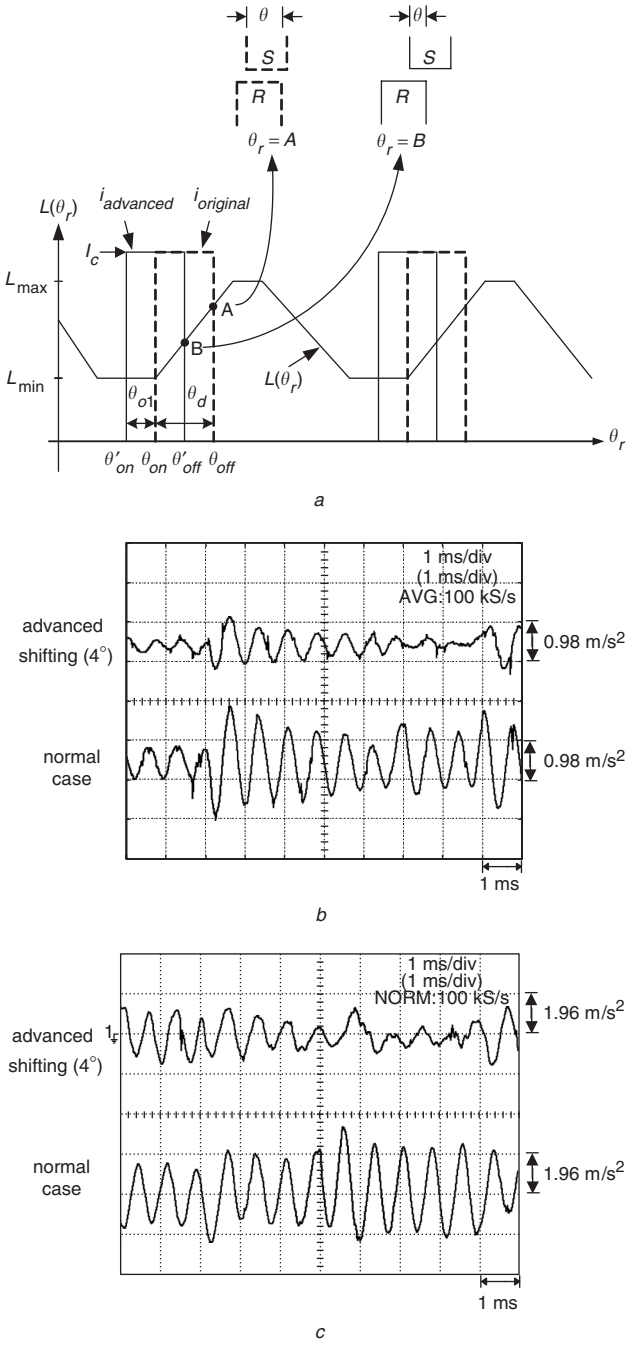

Fig. 6
a Idealised winding current and inductance profiles before and after commutation advanced shift
b Measured stator accelerations at $\omega_r = 700$ rpm, $R_L = 158\,\Omega$ without and with advanced shift of 4°
c Measured stator accelerations at $\omega_r = 1500$ rpm, $R_L = 104\,\Omega$ without and with advanced shift of 4°

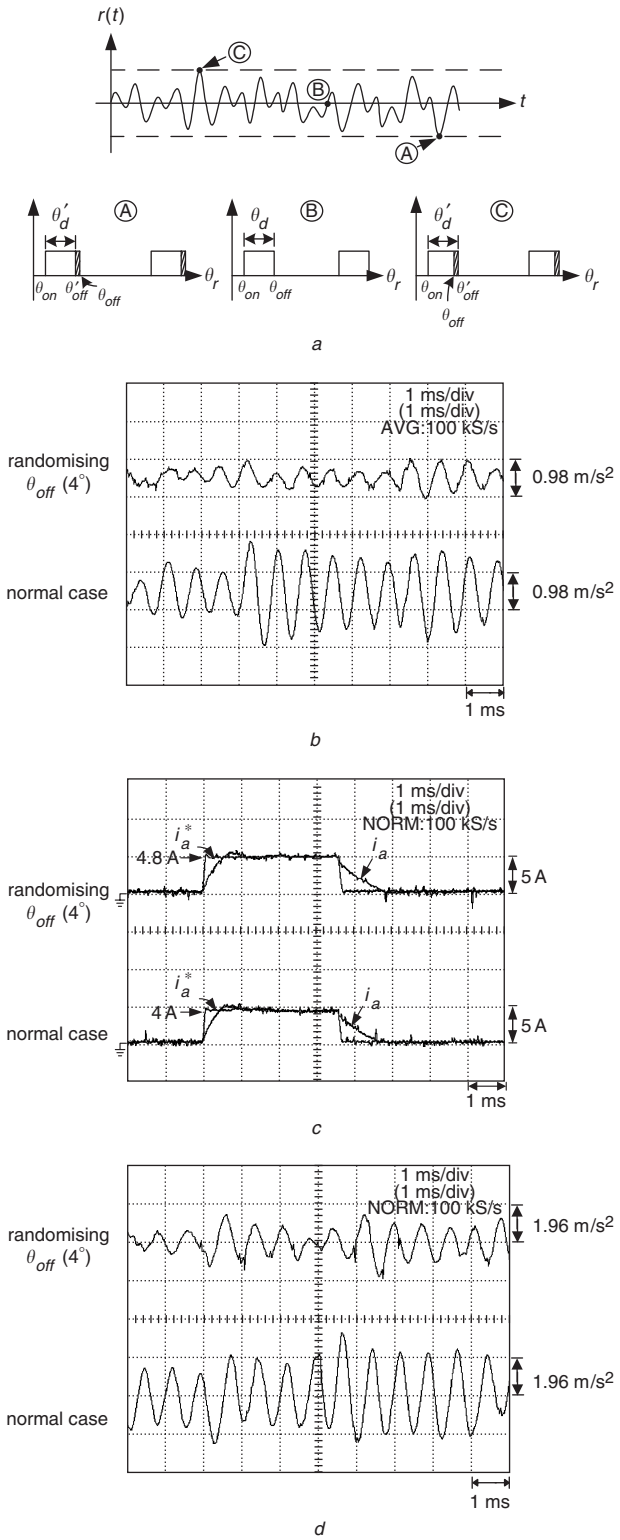

Fig. 7
a Employed random signal $r(t)$ and angles of θ'_{off} corresponding to $r(t) = A$, B and C
b Measured stator accelerations at $\omega_r = 700$ rpm, $R_L = 158\,\Omega$ without and with θ_{off} randomisation with $\Delta\theta = 4°$
c Measured winding currents and their commands corresponding to *b*
d Measured stator accelerations at $\omega_r = 1500$ rpm, $R_L = 104\,\Omega$ without and with θ_{off} randomisation with $\Delta\theta = 4°$

torque-generating capability. In addition, the effects of random signal attributes including magnitude and frequency range on the vibration and torque-generating capability are need to be studied deeply. In practice, for fixed θ_{on}, the randomisation of θ_{off} can easily be achieved by randomly changing the position register content, which stores the information of dwell angle θ_d.

At $\omega_r = 700$ rpm, $R_L = 158\,\Omega$, the measured stator accelerations for the normal case and θ_{off} randomisation with $\Delta\theta = 4°$ are compared in Fig. 7*b*. The corresponding measured winding currents and their commands are shown in Fig. 7*c*. The results in Figs. 7*b* and *c* show that the vibration has been reduced subject to slight increase in winding current from $I_c = 4.0$ to 4.8 A. Further experimental results indicate that, with the increase in extent of randomisation $\Delta\theta$, the vibration can be further decreased subject to a continuous increase in winding current. The measured accelerations at $\omega_r = 1500$ rpm, $R_L = 104\,\Omega$ shown in Fig. 7*d* also confirm the effectiveness of the proposed vibration reduction approach at higher speed.

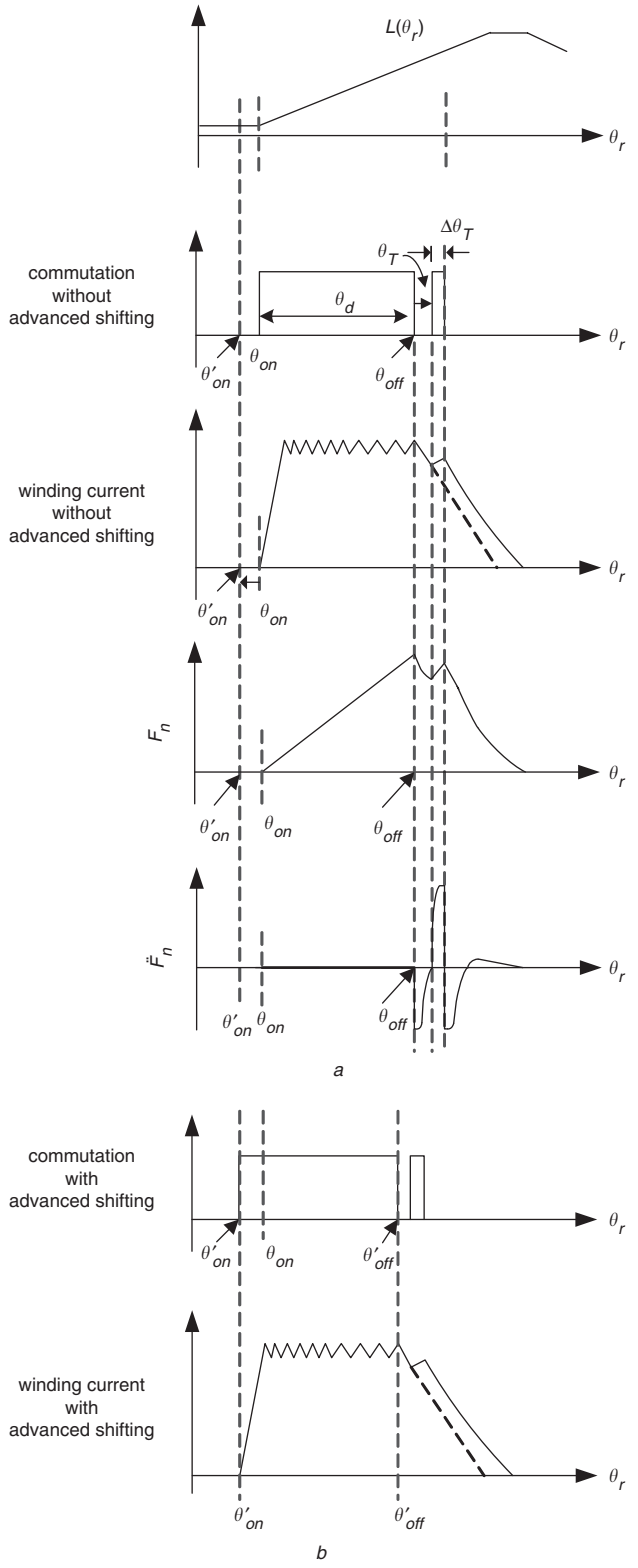

Fig. 8 *Proposed current-tail profiling control approaches*
a Inductance profile, commutation signal, winding current, F_n and $\ddot{F}_n$ without advanced commutation shift
b Commutation signal and winding current with advanced commutation shift

4.4 Current-tail profiling

To understand this control methodology, from (4) and (11) the radial force is expressed as:

$$F_n = \frac{-lr\mu_0 N^2}{2g^2}\theta i^2 \tag{19}$$

After demagnetisation at $\theta_r = \theta_{off}$, the vibration behaviour of the stator can be characterised by a second-order

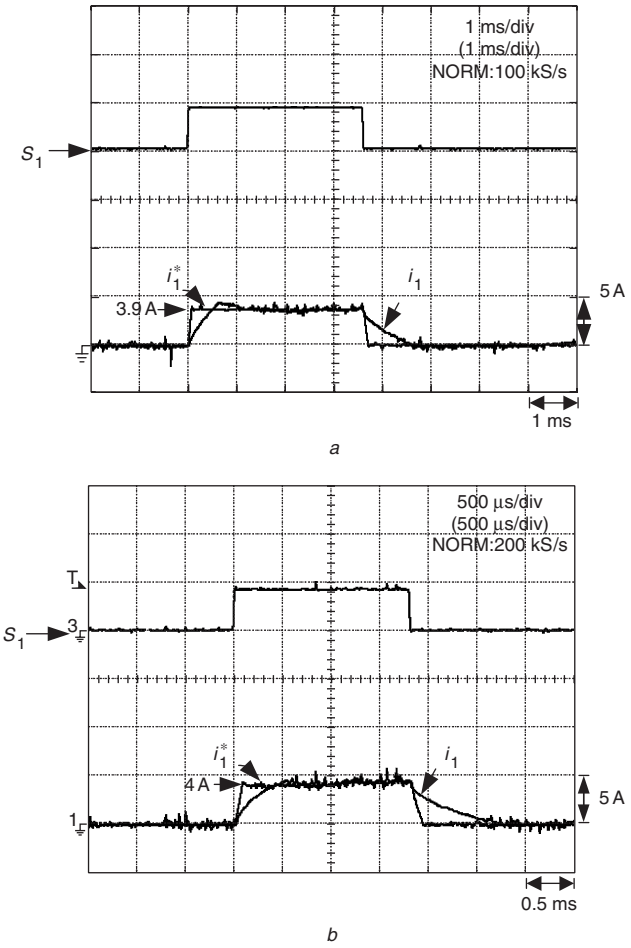

Fig. 9
a Measured winding current and its command for normal case (without making current-tail profiling) at $\omega_r = 700$ rpm, $R_L = 158\,\Omega$
b Same as *a* at $\omega_r = 1500$ rpm, $R_L = 104\,\Omega$

dynamic equation [9]:

$$\frac{\ddot{F}_n}{m} = \ddot{a} + 2\xi\omega_n\dot{a} + \omega_n a \tag{20}$$

where m = equivalent mass, a = vibration acceleration of stator, $\omega_n = \sqrt{k/m}$, $\xi = b/(2\sqrt{km})$, k = stiffness and b = viscous damping coefficient. From (19) and (20), one can see that the reduction of $\ddot{F}_n$ via smoothing of the winding current-tail is an effective remedy in vibration reduction. As mentioned previously, many existing methods can be applied. For example, one can apply a narrow pulse with proper width before the turn-off instant. This corresponds to the three-stage commutation method presented in [10]. Two types of current-tail profiling control approaches are studied in this paper.

4.4.1 Fixed commutation instant: The proposed current-tail profiling control approach without advanced shifting of the commutation instant is shown in Fig. 8*a*. A narrow pulse width $\Delta\theta_T$ behind the turn-off instant small angle θ_T is added to let the winding be re-excited by V_d with a narrow duration of $\Delta\theta_T$. It follows that the current-tail changing rate will become slower, as shown in Fig. 8*a*. The two tunable parameters in this approach are θ_T and $\Delta\theta_T$, which are dependent on the speed and loading condition, and they are determined by trial-and-error here. F_n and $\ddot{F}_n$ with added narrow pulse are also shown in Fig. 8*a*. The generation of the positive rectangular pulse in $\ddot{F}_n$ due to

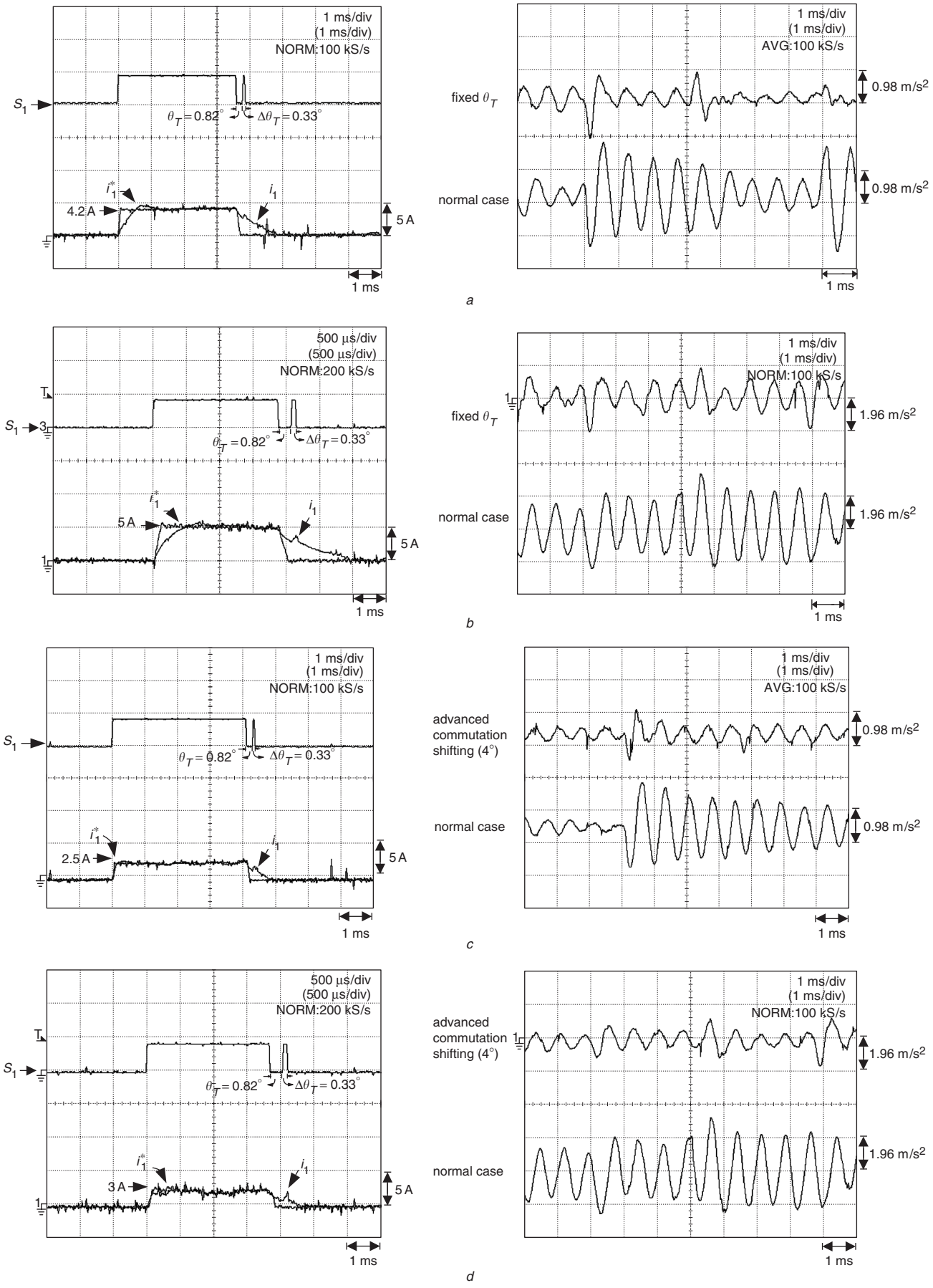

Fig. 10

a Measured winding current, its command and stator vibrations at $\omega_r = 700$ rpm, $R_L = 158\,\Omega$ by current-tail profiling with fixed $\theta_T = 0.82^\circ$ and $\Delta\theta_T = 0.33^\circ$

b Same as *a* at $\omega_r = 1500$ rpm, $R_L = 104\,\Omega$

c Same as *a* by advanced commutation shift of 4°

d Same as *c* at $\omega_r = 1500$ rpm, $R_L = 104\,\Omega$

current-tail profiling is helpful in the reduction of vibration [9, 10].

4.4.2 Advanced commutation instant: Although the current-tail profiling approach shown in Fig. 8*a* can be applied to reduce the axial force between stator and rotor, the long current-tail will reduce the developed torque. The proposed improved current-tail profiling approach is shown in Fig. 8*b*. By simultaneously advance shifting the whole switching pattern including the main and the auxiliary pulses, the generated negative torque can be reduced. It follows that the negative effects of current-tail profiling are compensated for.

4.4.3 Experimental results: *Fixed commutation instant*: For convenience of comparison, Figs. 9*a* and *b* show the winding currents and their commands without making current-tail profiling at $\omega_r = 700$ rpm, $R_L = 158\,\Omega$ and $\omega_r = 1500$ rpm, $R_L = 104\,\Omega$, respectively. Figures 10*a* and *b* show the winding currents and stator accelerations under current-tail profiling with $\theta_T = 0.82^\circ$ and $\Delta\theta_T = 0.33^\circ$. The results indicate that, by applying fixed current-tail profiling, the vibration is reduced at different motor speeds, but the winding currents are increased respectively from $I_c = 3.9$ to 4.2 A ($\omega_r = 700$ rpm, $R_L = 158\,\Omega$) and $I_c = 4.0$ to 5.0 A ($\omega_r = 1500$ rpm, $R_L = 104\,\Omega$).

4.4.4 Experimental results: *Advanced commutation instant*: Let the advanced commutation shift be 4°; the measured winding currents and accelerations at $\omega_r = 700$ rpm, $R_L = 158\,\Omega$ are shown in Fig. 10*c*. The measured results at a higher speed ($\omega_r = 1500$ rpm, $R_L = 104\,\Omega$) are shown in Fig. 10*d*. The results indicate that, through applying current-tail profiling with advanced commutation shift, both the current magnitudes (from 4.2 to 2.5 A for $\omega_r = 700$ rpm, from 5.0 to 3.0 A for $\omega_r = 1500$ rpm) and the stator vibrations are greatly reduced simultaneously. The reduction in winding current under the same load condition implies an increase in developed torque.

5 Comparative evaluation

Having performed the studies concerning five approaches in acoustic noise and vibration reduction, some observations and comments are now made. These five approaches are (i) RFPWM with harmonic spectrum shaping; (ii) simultaneously advanced θ_{on} and θ_{off} with fixed θ_d; (iii) randomising θ_{off}; (iv) current-tail profiling; and (v) current-tail profiling with advanced commutation shift.

These five approaches all can reduce the acoustic noise and vibration. Although the RFPWM approach is considered to be less effective until now and the related research is scarce, the application of the proposed spectrum shaping technique can improve this effectively. However, further studies to yield better results are still worth performing.

Among the five studied approaches, approaches (i) and (ii) can reduce vibration through the reduction of torque ripple and, moreover, the former can reduce the probability of the coincidence of current ripple frequencies with the stator resonant frequencies. As to approaches (iii) to (v), the radial force at turn-off and thus the vibration can be effectively reduced.

Current-tail profiling is very effective in acoustic noise and vibration reduction subject to an increase in the required winding current, i.e. a reduction in torque generating capability. However, by applying the proposed hybrid tuning approach, i.e. current-tail profiling with advanced commutation shift, good compromise performances in the increase of torque generating capability and the reduction of acoustic noise and vibration are obtained.

6 Conclusions

This paper has presented studies concerning reductions of acoustic noise and vibration of an SRM. A DSP-based SRM drive with properly mounted acceleration sensor is established and used as a test platform. Studies concerning the sources of acoustic noise and vibration find that the radial attraction force is the major reason, and effective magnetic and electronic remedies are also understood. Accordingly, this paper then proposed five mitigation approaches, including RFPWM with robust harmonic spectrum shaping, advanced turn-on and turn-off angles with fixed dwell angle, randomising turn-off angle, current-tail profiling, and current-tail profiling with commutation advanced shift. It has been found that, through applying the developed spectrum shaping technique, RFPWM can be made more effective in the reduction of acoustic noise and vibration. Current-tail profiling with advanced shift developed in this paper possesses the best compromise performance in the increase of torque generating capability and reduction of acoustic noise and vibration. Theoretical basis, design and implementation of all the proposed control schemes are described in detail, and the performance for all the schemes has been confirmed experimentally. In addition, the limits and key issues for further studies concerning all control approaches have also been considered.

7 Acknowledgment

The research was supported by the National Science Council, Taiwan, ROC, under the Grant of # NSC 93-2213-E-007-107.

8 References

1 Krishnan, R.: 'Switched reluctance motor drives: modeling, simulation, analysis, design, and applications' (CRC Press, New York, 2001)
2 Miller, T.J.E.: 'Optimal design of switched reluctance motors', *IEEE Trans. Ind. Electron.*, 2002, **49**, (1), pp. 15–27
3 Cameron, D.E., Lang, J.H., and Umans, S.D.: 'The origin of acoustic noise in variable-reluctance motors'. Proc. IEEE IAS Conf., 1989, Vol. 1, pp. 108–115
4 Cameron, D.E., Lang, J.H., and Umans, S.D.: 'The origin and reduction of acoustic noise in doubly salient variable-reluctance motors', *IEEE Trans. Ind. Appl.*, 1992, **28**, (1), pp. 1250–1255
5 Colby, R.S., Mottier, F.M., and Miller, T.J.E.: 'Vibration modes and acoustic noise in a four-phase switched reluctance motor', *IEEE Trans. Ind. Appl.*, 1996, **32**, (2), pp. 1357–1364
6 Gabsi, M., Camus, F., Loyau, T., and Barbry, J.L.: 'Noise reduction of switched reluctance machine'. Proc. IEEE IEMD Conf., 1999, pp. 263–265
7 Cai, W., Pillay, P., Tang, Z., and Omekanda, A.: 'Experimental study of vibrations in the switched reluctance motor'. Proc. IEEE IEMD Conf., 2001, Vol. 1, pp. 576–581
8 Fahimi, B., Suresh, G., Rahman, K.M., and Ehsani, M.: 'Mitigation of acoustic noise and vibration in switched reluctance motor drive using neural network based current profiling'. Proc. IEEE IAS Conf., 1998, Vol. 1, pp. 715–722
9 Michaelides, A., and Pollock, C.: 'Reduction of noise and vibration in switched reluctance motors: new aspects'. IEEE Rec. IAS, 1996, Vol. 2, pp. 771–778
10 Pollock, C., and Wu, C.Y.: 'Acoustic noise cancellation techniques for switched reluctance drives', *IEEE Trans. Ind. Appl.*, 1997, **33**, (1), pp. 477–484
11 Pillay, P., and Cai, M.: 'An investigation into vibration in switched reluctance motors', *IEEE Trans. Ind. Appl.*, 1999, **35**, (3), pp. 589–596
12 Krishnan, R., and Vijayraghavan, P.: 'State of the art: acoustic noise in switched reluctance motor drives'. Proc. IEEE IECON Conf., 1998, Vol. 2, pp. 929–934
13 Blaabjerg, F., and Pedersen, J.K.: 'Digital implemented random modulation strategies for AC and switched reluctance drives'. Proc. IEEE IECON Conf., 1993, Vol. 2, pp. 676–682

14 Im, Y.C., Kim, K.H., Na, S.H., Kim, H.D., and An, J.H.: 'Reduce acoustic noise in SRM using RPWM'. Proc. Annual KIPE Conf., Korea, 1998, pp. 189–192
15 Boukhobza, T., Gabsi, M., and Grioni, B.: 'Random variation of control angles, reduction of SRM vibrations'. Proc. IEEE IEMD Conf., 2001, Vol. 3, pp. 640–643
16 Ahn, J.W., Park, S.J., and Lee, D.H.: 'Hybrid excitation of SRM for reduction of vibration and acoustic noise', *IEEE Trans. Ind. Electron.*, 2004, **51**, (2), pp. 374–380
17 Ha, K.H., Kim, Y.K., Lee, G.H., and Hong, J.P.: 'Vibration reduction of switched reluctance motor by experimental transfer function and response surface methodology', *IEEE Trans. Ind. Electron.*, 2004, **40**, (2), pp. 577–580
18 Cailleux, H., Pioufle, B.L., Multon, B., and Sol, C.: 'A precise analysis of the phase commutation for the torque nonlinear control of a switched reluctance motor – torque ripples minimization'. Proc. IEEE IECON Conf., 1993, Vol. 3, pp. 1985–1990
19 Lovatt, H.C., and Stephenson, J.M.: 'Computer-optimised smooth-torque current waveforms for switched-reluctance motors', *IEE Proc., Electr. Power Appl.*, 1997, **144**, (5), pp. 310–316
20 Chapman, P.L., and Sudhoff, S.D.: 'Optimized waveform control for an 8/6 switched reluctance motor drive'. Proc. IEEE APEC Conf., 2001, Vol. 2, pp. 1096–1102
21 Stephenson, J.M., Hughes, A., and Mann, R.: 'Torque ripple minimization in a switched reluctance motor by optimum harmonic current injection', *IEE Proc., Electr. Power Appl.*, 2001, **148**, (4), pp. 322–328
22 Stephenson, J.M., Hughes, A., and Mann, R.: 'Online torque-ripple minimization in a switched reluctance motor over a wide speed range', *IEE Proc., Electr. Power Appl.*, 2002, **149**, (4), pp. 261–267
23 Liaw, C.M., and Lin, Y.M.: 'Random slope PWM inverter using system existed background noise: analysis, design and implementation', *IEE Proc., Electr. Power Appl.*, 2000, **147**, pp. 45–54
24 Kang, B.J., and Liaw, C.M.: 'Random hysteresis PWM inverter with robust spectrum shaping', *IEEE Trans. Aerosp. Electron. Syst.*, 2001, **37**, (2), pp. 619–629
25 Mademlis, C., and Kiosderidis, I.: 'Performance optimization in switched reluctance motor drives with online commutation angle control', *IEEE Trans. Energy Convers.*, 2003, **18**, (3), pp. 448–457